PHOTONICS Research

Machine learning-based analysis of multiple simultaneous disturbances applied on a transmission-reflection analysis based distributed sensor using a nanoparticle-doped fiber

Letícia Avellar,[1] Anselmo Frizera,[1] Helder Rocha,[1] Mariana Silveira,[1] Camilo Díaz,[1] Wilfried Blanc,[2] Carlos Marques,[3,*] and Arnaldo Leal-Junior[1]

[1]Graduate Program of Electrical Engineering, Federal University of Espirito Santo, Vitoria 29075-910, Brazil
[2]Université Côte d'Azur, Institut de Physique de Nice, CNRS, 06108 Nice Cedex 2, France
[3]I3N and Physics Department, Universidade de Aveiro, Campus Universitário de Santiago, Aveiro 3810-193, Portugal
*Corresponding author: carlos.marques@ua.pt

Received 22 July 2022; revised 6 December 2022; accepted 6 December 2022; posted 9 December 2022 (Doc. ID 471301); published 9 February 2023

Photonic technology combined with artificial intelligence plays a key role in the development of the latest smart system trends, integrating cutting-edge technology with machine learning models. This paper proposes a transmission-reflection analysis based system using dielectric nanoparticle-doped fiber combined with artificial intelligence to address one of the major problems in the distributed sensing approach: reducing the cost while maintaining high spatial resolution to close the gap between distributed sensors and the general public. Machine learning-based models are designed to classify the perturbed positions when the same force is used and force regression when different forces are applied on each position. The results show an accuracy of 99.43% in the position classification of multiple disturbances and an rms error of 1.53 N in the force regression, which represents 5% of the force range. In addition, a smart environment using the current system is proposed, which presented 100% accuracy in identifying the positions of different persons in the environment. This smart environment enables remote home care of patients with high reliability, intelligent decision-making, and a predictive capability.

https://doi.org/10.1364/PRJ.471301

1. INTRODUCTION

The Internet of Things (IoT) has revolutionized the global world by enabling interconnection between several smart devices through wireless communications [1,2]. Photonic-based technology is a potential alternative for next-generation communications systems, which could deliver very high-speed, reliable data transmission. For next-generation sensor systems, photonics-based sensors also offer multiplexing and miniaturization capabilities, especially as a solution for the challenges of IoT technology [3,4]. As an IoT strand, smart cities enable novel technologies to be interconnected to provide high-quality basic services through relevant information, improving the quality and lifestyle of city residents [5]. This concept covers transportation, healthcare, and personal homes/offices [6].

Digital health can be defined as the intersection between digital technology and healthcare services, which includes digital information, data, and communications technologies to collect, share, and analyze health information [7]. The widespread use of digital health technologies has increased in the medical field, motivated by the aging population [8]. When combined with artificial intelligence (AI) technology, digital health technologies can improve diagnosis, treatment, clinical decision support, and care management. In addition, digital health technologies can be scaled to reach thousands of people, which can improve both the clinical health status of patients [9] and healthcare delivery [10], while also reducing the cost of care [7].

The fusion of emerging AI technology with photonic sensors has promoted a new era of intelligent sensing, mitigating impairments in optical systems and resulting in a technology able to perform a more complicated and comprehensive analysis [11]. From physics-inspired optical designs, the future is heading toward data-driven designs that will change both optical hardware and next-generation software systems [12].

Regarding current photonic sensing technology, optical fiber sensors (OFSs) present several intrinsic advantages: OFSs are lightweight, compact, chemically stable, immune

to electromagnetic fields and have multiplexing capabilities [13,14]. OFSs are also compatible with the requirements of IoT technology [15], which mainly relies on the wireless connectivity of several miniaturized sensors that offer low energy consumption [16]. The combination of OFS and IoT technologies has had a major impact on the concept of digital health [17,18]. This combination has the potential to produce better outcomes for patients, by providing intelligent health data analytics and guaranteeing preventive medicine and care for the elderly [8], since these sensor systems allow the continuous monitoring of patients' activities [17], which results in remote assistive services, early detection of health issues, and transport in case of emergencies [19].

OFS can be classified based on spatial positioning, in which the sensors can measure punctually or along the fiber [20]. This classification is divided into three types: punctual, quasi-distributed, or distributed sensors. Punctual sensors provide the value of a physical parameter of interest locally [21], whereas distributed sensors provide the value of a physical parameter over a distance and as a function of the position along the fiber [22]. In quasi-distributed sensors [23], such as the fiber Bragg grating (FBG) sensor systems [24], the variable is measured at discrete points along the fiber.

A distributed OFS is a very attractive approach to locate loss-inducing perturbations along the fiber [25]. The backscattering-based sensing technology is often employed for the localization of a loss-inducing perturbation, in which the two main methods are optical time domain reflectometry (OTDR) [26] and optical frequency domain reflectometry (OFDR) [27]. However, these methods use modulated light sources and demand interrogation systems that are complex and costly [28], which make them impractical for massive deployment and unavailable for the general public.

Transmission-reflection analysis (TRA) is a simple, inexpensive technique developed to locate loss-inducing perturbation based on measurement of the transmitted and backscattered powers of an unmodulated light source [29,30]. Despite its simplicity and low cost, the TRA technique is developed for single perturbation tracking and presents poor spatial resolution (~m) when applied to standard silica fibers due to a low Rayleigh backscattering signal [31,32]. An alternative to increase the Rayleigh backscattering power is using silica optical fibers containing oxide nanoparticles, so-called dielectric nanoparticles-doped (DNP-doped) fibers [33]. The DNP-doped high scattering fibers are an attractive solution to enhance the spatial resolution of TRA-based systems [34], such as presented in Ref. [32], which reported an improvement in the spatial resolution using a MgO-doped fiber (spatial resolution in mm).

The cost reduction of distributed OFSs can be useful for applications in fields such as healthcare that involve the general public. To achieve a low-cost distributed system with a spatial resolution of cm, this paper presents the combination of a TRA-based sensor using DNP-doped fiber and AI algorithms, resulting in an AI-integrated optical fiber sensing approach, as shown in Fig. 1. Classification and regression neural network models are designed to characterize the system under multiple simultaneous disturbances using the same (or different) forces.

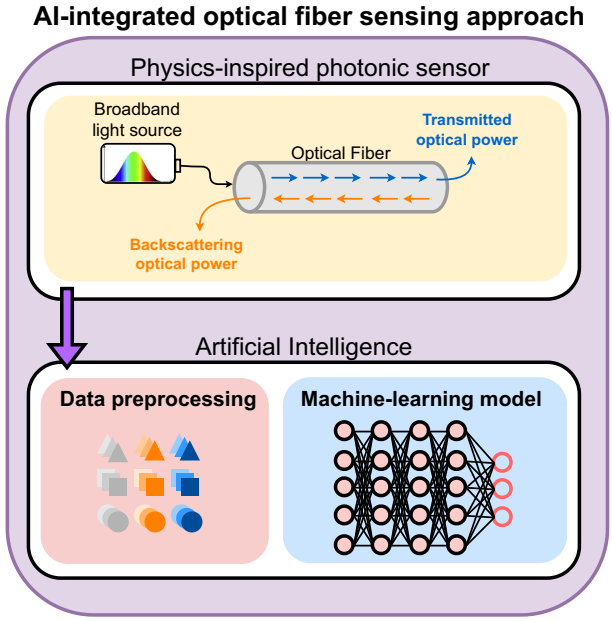

Fig. 1. AI-integrated optical fiber sensing approach as a result of the combination of a photonics sensor and machine learning.

Furthermore, to validate the proposed system in a healthcare application and to close the gap between distributed sensing technology and the general public, the system is embedded in a room simulating a small house to evaluate its ability to identify the position of different people in the environment, resulting in cutting-edge technology accessible to the general population.

2. MATERIALS AND METHODS

The materials used in this setup are divided into three parts: the light source, the acquisition system, and the optical fibers. The superluminescent diode (SLED) centered at 1550 nm with a bandwidth of 60 nm (DL-BP1-1501A, Ibsen Photonics, Farum, Denmark) was employed as the light source. The acquisition system consists of two photodetectors (PDs; GT322D, Go4fiber Ltd., Hong Kong, China), two transimpedance amplifiers (TIAs; TLV3541, Texas Instruments, Dallas, USA), a microcontroller unit (MCU; Kinetis K25Z, NXP Semiconductors, Eindhoven, the Netherlands), and a computer. An optical circulator (OC) is employed to connect the reflected optical power to one PD, whereas the other PD is directly connected at the optical fiber to acquire the transmitted optical power. Each PD is coupled to the TIAs and the signal acquisition is performed by the microcontroller and transmitted to the computer for data processing.

The fiber used in this setup is a DNP-doped fiber, which is fabricated following the guidelines presented in Ref. [35]. The standard solution doping technique is used to incorporate Mg ions, which trigger the formation of Mg-silicate nanoparticles during the modified chemical vapor deposition (MCVD) process, and Er ions, which are mainly located in the nanoparticles. In addition, germanium (1.85%, molar fraction) and small amounts of phosphorus (0.8%, molar fraction) were added

to raise the core refractive index and ease the fabrication of these fibers. It is important to mention that no particle bigger than 100 nm was observed in this fiber.

A. System Characterization

Two experimental protocols were performed to characterize the system under multiple simultaneous disturbances. These protocols are performed to evaluate the transmitted and reflected optical power when disturbances are applied simultaneously on different points along the 150 cm long fiber. Protocol 1 consists of different combinations of disturbances using the same force, including single and multiple simultaneous perturbations. Six points are defined, separated by 15 cm. The goal of this characterization is to identify the disturbance points (when the same force is applied) by analyzing the transmitted and reflected optical powers. Protocol 2 consists of different combinations of multiple disturbances using different forces and the same points of Protocol 1. Figure 2 presents the experimental setup of the characterization.

Since new data do not depend on past elements in this application, the selected machine learning algorithm was the feedforward neural network (FFNN), which is generalized and simple to train with full connectivity between adjacent layers. Two FFNN models were designed, as shown in Fig. 3, by analyzing the transmitted and reflected powers (input): one to classify the disturbance event at six predefined points and the other to model a force regression for each predefined point, which can identify which point was disturbed and which force was applied on each point.

Two hidden layers, hidden layer 1 and hidden layer 2, were included with, respectively, 600 and 300 neurons after empirical validation. The activation function used in the hidden layers was the rectified linear activation function (ReLU), whereas the activation function used in the output layer is the sigmoid for Protocol 1, since it is a multilabel classification, and linear for Protocol 2. The data is divided into training (80%) and testing (20%), and randomly permuted. Also, the input data (transmitted and reflected powers) are normalized between −1 and 1. The mean squared error (MSE) is used as a loss for both protocols. For Protocol 1, accuracy is used as the classification metric. Moreover, confusion matrices are calculated for different trials (10) with the data randomly permuted. For Protocol 2, root mean square error (RMSE) is used as the regression metric.

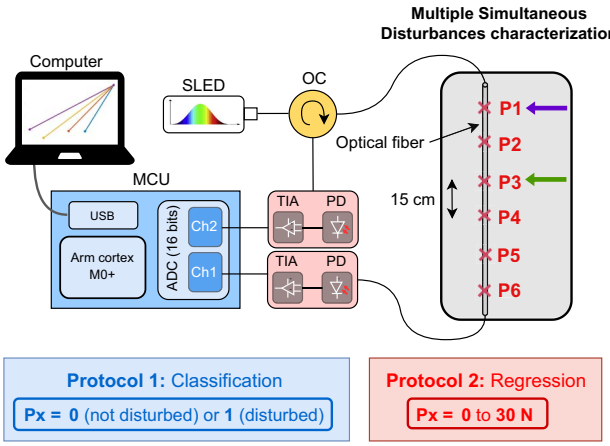

Fig. 2. Experimental setup of the multiple simultaneous disturbances characterization for two protocols.

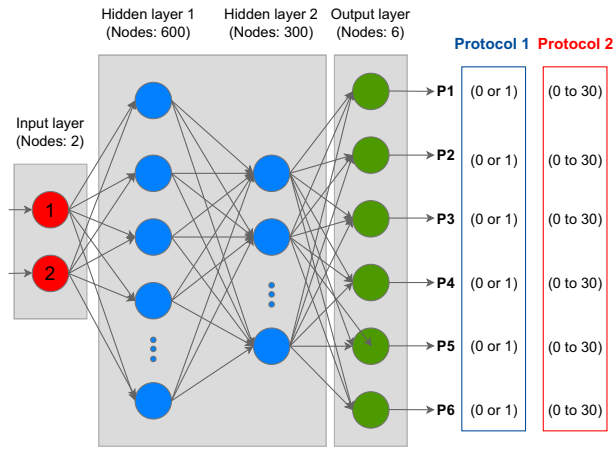

Fig. 3. FFNN model for both protocols of system's characterization.

The disturbances combination of Protocol 1 is presented in Table 1, where 1 represents a disturbance at the respective point (Px, $1 \leq x \leq 6$) and 0 represents no disturbance at the point. In the same way, Table 2 presents the combination of different and simultaneous forces (N) applied on the same points Px.

B. Smart Environment Based on the Proposed System

A 6 m × 6 m room, simulating a small house, is instrumented with the proposed system. Thus, the smart environment

Table 1. Combination of the Multiple Simultaneous Disturbances in Protocol 1 (Disturbance Classification)

Combination	P1	P2	P3	P4	P5	P6
1	1	0	0	0	0	0
2	0	1	0	0	0	0
3	0	0	1	0	0	0
4	0	0	0	1	0	0
5	0	0	0	0	1	0
6	0	0	0	0	0	1
7	1	1	0	0	0	0
8	1	0	1	0	0	0
9	1	0	0	1	0	0
10	1	0	0	0	1	0
11	1	0	0	0	0	1
12	0	1	1	0	0	0
13	0	1	0	1	0	0
14	0	1	0	0	1	0
15	0	1	0	0	0	1
16	0	0	1	1	0	0
17	0	0	1	0	1	0
18	0	0	1	0	0	1
19	0	0	0	1	1	0
20	0	0	0	1	0	1
21	0	0	0	0	1	1
22	1	1	1	0	0	0
23	0	1	1	1	0	0
24	0	0	1	1	1	0
25	0	0	0	1	1	1

Table 2. Combination of Different and Simultaneous Weights in Protocol 2 (Force Regression in Newtons)

Combination	P1	P2	P3	P4	P5	P6
1	10	0	0	0	0	0
2	20	0	0	0	0	0
3	0	10	0	0	0	0
4	0	20	0	0	0	0
5	0	0	10	0	0	0
6	0	0	20	0	0	0
7	0	0	0	10	0	0
8	0	0	0	20	0	0
9	0	0	0	0	10	0
10	0	0	0	0	20	0
11	10	0	10	0	0	0
12	10	0	20	0	0	0
13	10	0	30	0	0	0
14	10	0	0	0	10	0
15	10	0	0	0	20	0
16	10	0	0	0	30	0
17	20	0	10	0	0	0
18	30	0	10	0	0	0
19	0	0	10	0	10	0
20	0	0	10	0	20	0
21	0	0	10	0	30	0

comprises six principal places: entrance carpet, chair, bathroom handrail, bedroom carpet, bed, and desktop, as shown in Fig. 4. The DNP-doped fiber (20 m length) is incorporated in all these places. In the TRA setup, which is presented in the Section 2.A, the transmitted and reflected optical powers indicate the position of the person in the environment, since previous results showed the ability to identify the disturbance location in the fiber. In this way, the smart environment protocol is divided into two parts. The first part consists of one person accessing all the predefined places (locations) sorted in ascending order (L1 to L6) while the transmitted and reflected optical powers are acquired. The second part consists of two persons randomly accessing different places.

For the smart environment protocol, an FFNN classification model is also designed to identify the places in the house the person (or persons) accessed using the transmitted and reflected optical powers as the input data, as previously shown. The data are divided into training (80%) and testing (20%), and are associated with their respective classes (places). The input data are normalized between −1 and 1. The FFNN model is evaluated by the accuracy and loss (MSE). With the designed model, it is possible to perform the online classification of new data.

3. RESULTS AND DISCUSSION

A. System Characterization

The normalized transmitted and reflected optical powers are the input 1 and input 2 of the FFNN model, as shown in Fig. 3, which pass through two hidden layers and then result in the outputs; i.e., the disturbance classification (Protocol 1) or the force regression (Protocol 2) among the six possible positions. These approaches (both protocols) address a critical drawback in TRA-based systems; i.e., the issue of assessing simultaneous perturbations along the fiber. Conventionally, TRA-based systems use the transmission and reflection data

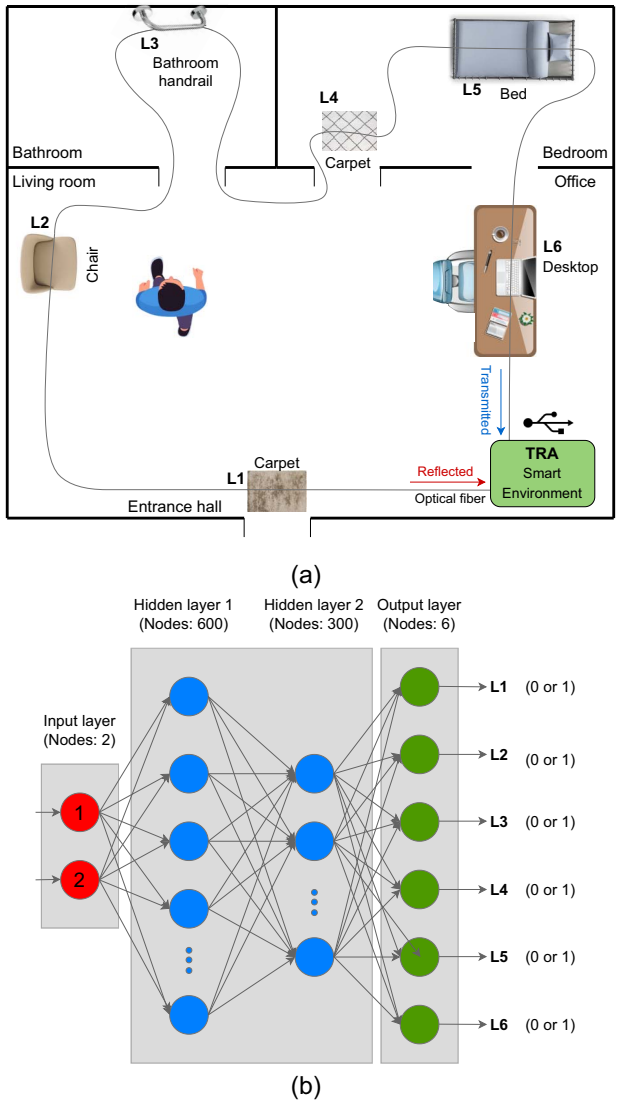

Fig. 4. Smart environment protocol. (a) Smart environment setup: entrance carpet (L1), chair (L2), bathroom handrail (L3), bedroom carpet (L4), bed (L5), and desktop (L6). (b) FFNN model for the smart environment protocol.

to estimate the position of a mechanical perturbation in the fiber, and the use of this approach in conjunction with machine learning enables the detection of multiple perturbations (up to three simultaneous perturbations, in this case) along the optical fiber. Furthermore, the spatial resolution of 15 cm is obtained, which is the distance between two consecutive classification regions and it comprises a length smaller than the length of a human foot. Figure 5 shows the transmission and reflection optical powers for three cases during Protocol 1 (using the same force): single-point perturbation, two-point perturbation, and three-point perturbation.

In Protocol 1, the results in Fig. 5 show that both the reflected and transmitted optical powers varied with the position and number of perturbations along the fiber. Thus, the use of the FFNN classification model enables the correct classification of each perturbation, even when multiple perturbations are

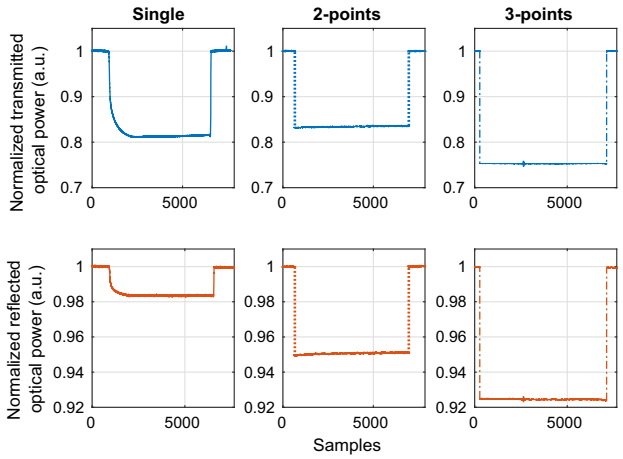

Fig. 5. Transmitted and reflected optical powers under three conditions in Protocol 1: (a) single-point perturbation, (b) two-point perturbation, and (c) three-point perturbation.

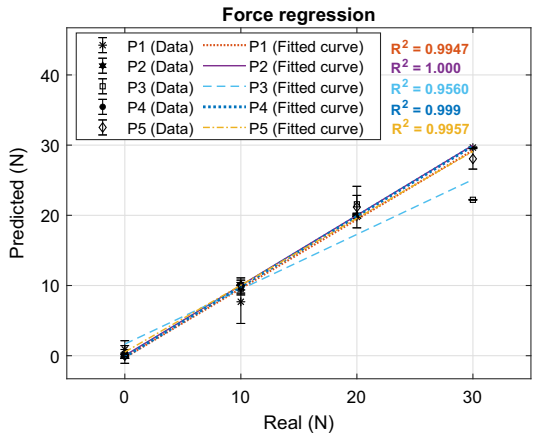

Fig. 7. Results of the force regression for each point (no weight was applied on P6).

applied in the DNP-doped optical fiber. Results of the FFNN classification model showed that the accuracy value converged to 99.43% and the loss (MSE) value to 0.0144 for 40 epochs. Such results indicate the suitability of the proposed approach for multiple impact classification, in which the high accuracy indicates negligible errors in the perturbation detection. To verify the classification at each position, Fig. 6 shows the confusion matrices (for each label/position) for single and multiple perturbation detection using deep learning/TRA-based systems. At each position, the classification was approximately 99% or more, in which the positions P2, P4, and P6 presented 100% accuracy. The misclassified samples may be related to mechanical deviations during the Protocol 1 experiment.

In Protocol 2, results of the FFNN regression model metrics showed that the RMSE value converged to 1.53 N and the loss (MSE) value to 0.17 N for 200 epochs. It represents 5% and 0.5%, respectively, of the total force range employed in this experiment. Also, for each position the real and predicted forces were compared, as presented in Fig. 7.

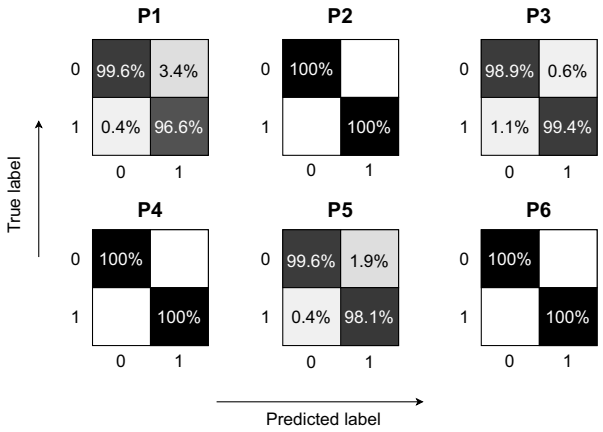

Fig. 6. Confusion matrices of each label for single and multiple perturbation detection using the FFNN model.

The results showed a coefficient of determination (R^2) higher than 0.99 and an RMSE approximately 1 N or lower for positions P1, P2, P4, and P5. At position P3, when the force was 30 N, the FFNN regression model presented errors, which resulted in an R^2 of 0.956 and an RMSE of 2.68 N. Since only the results referring to this position presented worse performance, it may be related to errors during the force application on this position. The results also may improve with an increase in the dataset for each condition; i.e., more experiments can reach better regression model performance. In addition to the errors due to the force application positioning in the optical fiber (such as perpendicularity and lateral displacements, which lead to a reduction in the force transmitted to the optical fiber), there are errors due to the nonlinearities in the sensor responses in some locations along the fiber. Such nonlinear responses can be related to nonuniformities on the nanoparticle distribution along the optical fiber length and diameter. It is also worth mentioning that such errors can be reduced if nonlinear models are used on the regression of P3. However, for comparison purposes, we presented the same model (linear regression) for all sensors to compare their linearity from the R^2.

Finally, Fig. 8 presents the temporal analysis of the forces applied on each position during Protocol 2. The continuous line represents the real force, whereas the dotted line represents the force predicted by the regression model. It is possible to observe a similarity between the curves. P1 presents a prediction curve similar to the real one during almost the entire test. However, when a force of 30 N is applied at position P3, the neural network model confuses P3 with P1, which leads to errors in these prediction curves. It may be an error in the regression model design due to similar inputs for P1 and P3. These punctual errors could be improved with an increase in the force range employed in this protocol and a bigger dataset.

B. Smart Environment Based on the Proposed System

Figure 9 presents the results of the transmitted and reflected optical powers during the smart environment protocol. The data are normalized by the results of the unstrained fiber.

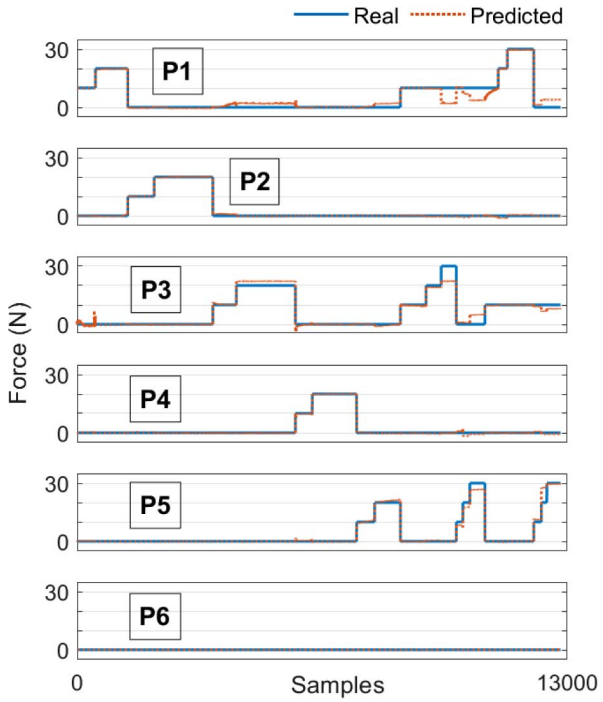

Fig. 8. Temporal analysis of real and predicted forces applied on each position.

It is possible to identify the events in which the volunteer accesses the locations ordered in Fig. 4, which was previously presented in Section 2.B. The first location (L1, entrance carpet) is the nearest point to the reflection photodetector, whereas the last location (L6, desktop) is the farthest one. It leads to a higher reflected optical power variation for locations closer to this photodetector, as presented in Fig. 9. Thus, if the force is applied close to the location L1, for example, there will be a variation similar to the one obtained at around 1000 samples (as presented in the bottom graph of Fig. 9), since the reflected optical power is proportional to the perturbation location, which is used as the main mechanism for perturbation location detection. For this reason, if the perturbation location is set as a constant distance to the reflection photodetector, the normalized reflected optical power will present the same variation due to the sensor's repeatability.

The transmitted optical power is related to the force applied on the optical fiber, whereas the reflected optical power is related to the location of this force. The disturbance points of each place require different forces; i.e., on the carpets, the force applied on the fiber is proportional to the volunteer's weight, whereas, on the bathroom handrail, the force can vary with a user's need to control his/her balance. For this reason, the transmitted optical power variation does not present a pattern. On the other hand, the reflected optical power variation decreases as the distance from the reflection photodetector increases. This is because the fiber length is longer, which leads to a weaker reflected signal than when using shorter fiber lengths. Thus, there is a higher reflected optical power variation in location L1, since it is closer to the reflection photodetector than location L6. It is worth emphasizing that the reflection optical power variation decreases as a function of the distance between the mechanical perturbation point and the reflection photodetector.

The results of the FFNN model are presented in Fig. 10. The accuracy and the loss converged, respectively, to approximately 100% and 0.01. The convergence of the model to an

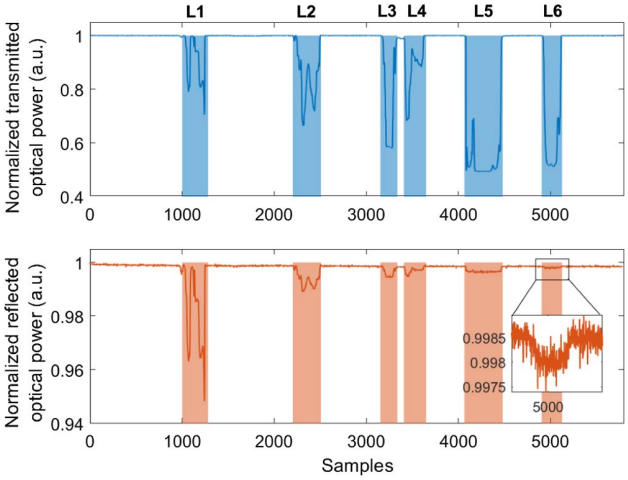

Fig. 9. Results of transmitted and reflected optical power using the TRA setup for place identification in the smart environment.

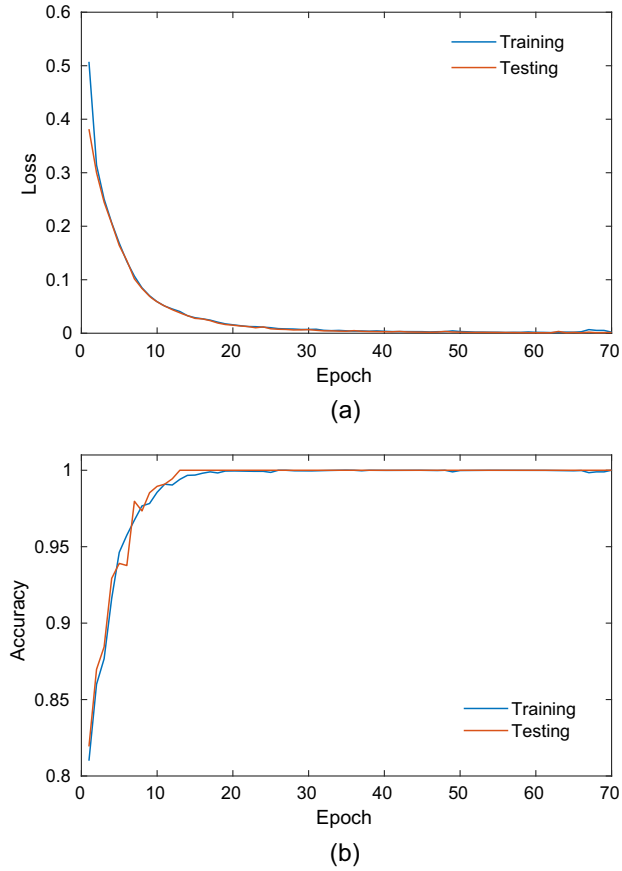

Fig. 10. Metrics of the FFNN model with 70 epochs for the identification of the accessed places in the smart environment: (a) loss and (b) accuracy.

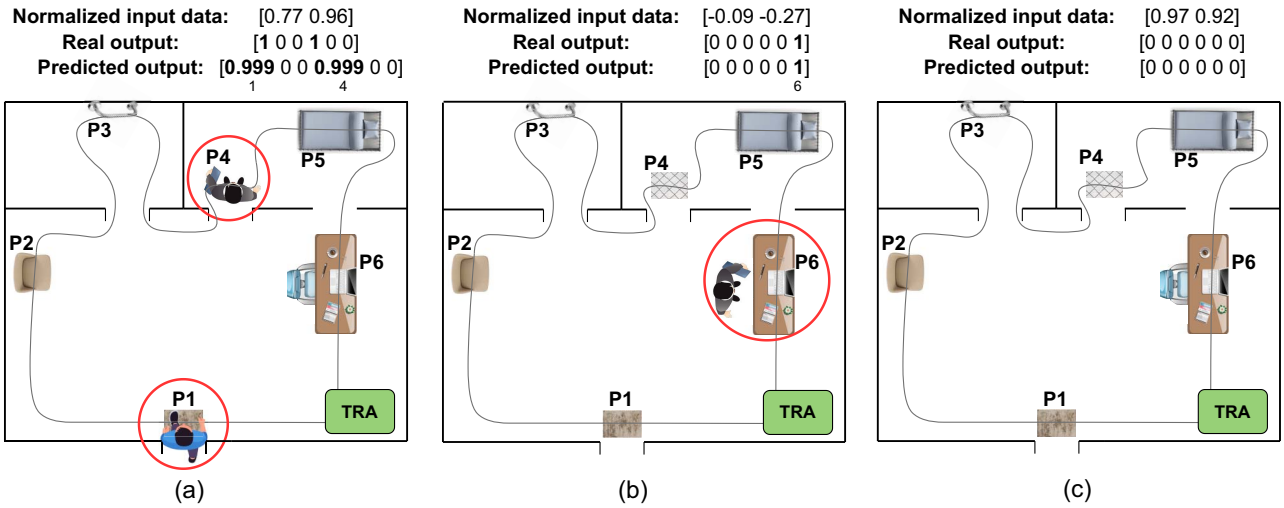

Fig. 11. Results of the classification of new data using the designed FFNN model for three different conditions: (a) two persons at home, (b) one person at home, and (c) no person at home.

accuracy of 100% represents the ability to identify the places that the person (or two persons) accessed. This identification can be processed online, and it allows remote monitoring by clinicians located in hospitals with high accuracy.

Based on the results of the classification metrics, the FFNN model can be used as the classifier of new data and can help identify the places accessed. Figure 11 presents an example of the result of the new data classification using the designed FFNN model. The input data are normalized between −1 and 1, as previously mentioned, and the first value corresponds to the transmitted optical power, whereas the last value corresponds to the reflected optical power. The real output consists of binary numbers in which 1 represents the case when a place is accessed and 0 represents the case when no place is accessed. The predicted output is the result of the FFNN model based on an input sample and corresponds to the probabilities of each class. These probabilities are rounded for accuracy estimation.

Different results were achieved using other machine learning algorithms to classify events in distributed sensing. Table 3 presents the comparison between different outcomes of researchers in the literature. It is important to notice that the OFS techniques mentioned in Table 3 are distributed sensing approaches, whereas TRA is a single-event technique. Thus, the results achieved in this paper enable the application of low-cost TRA-based sensors to detect multiple and simultaneous events as an alternative to high-cost distributed sensing approaches.

Table 3. Comparison of Outcomes Using Different Machine Learning Algorithms to Classify Events in Distributed Sensing

Ref.	Algorithm	OFS	Accuracy
[36]	ANN	OFDR	94.00%
[37]	SVM	Φ-OTDR	94.17%
[38]	CNN	Φ-OTDR	96.67%
[39]	CNN-LSTM	MZI	97.00%
This paper	FFNN	TRA	99.43%

4. CONCLUSION

This study presents the development and performance analysis of a low-cost multiple disturbance tracking system based on the combination of DNP-doped fiber, the TRA technique, and AI algorithms. A machine-learning-based analysis of multiple simultaneous disturbances applied on a TRA-based distributed sensor using a DNP-doped fiber was performed to address one of the major problems in the TRA-based approach; i.e., the ability to detect simultaneous perturbations along the optical fiber. The results showed an accuracy of 99.43% in the detection of single-point, two-point, and three-point perturbations (using the same force), which demonstrate the ability to identify the location of multiple simultaneous disturbances. The results of experiments using different forces during two-point perturbation also presented an RMSE of 1.53 N and R^2 higher than 0.95 between real and predicted forces. These preliminary studies showed the ability not only to identify the disturbance location but also to identify which force was applied to each location, enabling the development of distributed sensors with a low-cost technique as an alternative to costly distributed sensing methods. Finally, in the smart environment application, the results showed an accuracy of 100% in the identification of the position of different persons in the environment. These results validate the use of the proposed system as a remote healthcare service to continuously monitor patients, which enables intelligent decision-making. Thus, we believe that using an AI-integrated OFS for low-cost remote distributed monitoring can provide novel applications for distributed OFSs for widespread use in the general public and lead to applications that involve low-cost sensing approaches that are not yet covered by distributed OFSs. In addition, the decision-making can be generalized or improved for diagnosis not only of the physical conditions, but also for indirect emotional aspects of a user based on their daily routine and activities. There are, however, two major limitations in this study that can be addressed in future research. First, the study focused on six points along the fiber with a maximum of three

points of simultaneous disturbances for the proof of concept. Second, the maximum fiber length used in this work was 20 m, and it was possible to observe that the farthest point from the reflection photodetector already presented low optical power. Future tests will involve adding points and more simultaneous perturbations to improve the system's robustness. In addition, future tests also will include fibers longer than 20 m to evaluate the relationship between the fiber length and the system performance. Finally, future work will involve the use of the proposed system in smart environments for clinical validation with patients.

Funding. Coordenação de Aperfeiçoamento de Pessoal de Nível Superior (309737/2021-4, 310668/2021-2, 310709/2021-0, 84336650, 2021-WMR44, 304049/2019–0); Financiadora de Estudos e Projetos (2784/20); Agence Nationale de la Recherche (ANR-17-CE08-0002); Fundação para a Ciência e a Tecnologia (2021.00667.CEECIND, PTDC/EEI-EEE/0415/2021, UIDB/50025/2020, UIDP/50025/2020).

Acknowledgment. The authors acknowledge S. Trzesien and M. Ude (INPHYNI, Nice, France) for the fabrication of the fiber sample. Carlos Marques acknowledges the FCT.

Disclosures. The authors declare no conflicts of interest.

Data Availability. Data underlying the results presented in this paper are not publicly available at this time but may be obtained from the authors upon reasonable request.

REFERENCES

1. G. A. Akpakwu, B. J. Silva, G. P. Hancke, and A. M. Abu-Mahfouz, "A survey on 5G networks for the Internet of Things: communication technologies and challenges," IEEE Access **6**, 3619–3647 (2017).
2. A. Burg, A. Chattopadhyay, and K. Y. Lam, "Wireless communication and security issues for cyber–physical systems and the Internet-of-Things," Proc. IEEE **106**, 38–60 (2018).
3. S. R. Teli, S. Zvanovec, and Z. Ghassemlooy, "Optical Internet of Things within 5G: applications and challenges," in *2018 IEEE International Conference on Internet of Things and Intelligence System (IOTAIS)* (2018), pp. 40–45.
4. C. A. R. Díaz, C. Leitão, C. A. Marques, N. Alberto, M. F. Domingues, T. Ribeiro, M. J. Pontes, A. Frizera, P. F. Antunes, P. S. André, and M. R. Ribeiro, "IOTOF: a long-reach fully passive low-rate upstream PHY for IoT over fiber," Electronics **8**, 359 (2019).
5. E. Manavalan and K. Jayakrishna, "A review of Internet of Things (IoT) embedded sustainable supply chain for industry 4.0 requirements," Comput. Ind. Eng. **127**, 925–953 (2019).
6. K. Shafique, B. A. Khawaja, F. Sabir, S. Qazi, and M. Mustaqim, "Internet of Things (IoT) for next-generation smart systems: a review of current challenges, future trends and prospects for emerging 5G-IoT scenarios," IEEE Access **8**, 23022–23040 (2020).
7. A. Sharma, R. A. Harrington, M. B. McClellan, M. P. Turakhia, Z. J. Eapen, S. Steinhubl, J. R. Mault, M. D. Majmudar, L. Roessig, K. J. Chandross, E. M. Green, B. Patel, A. Hamer, J. Olgin, J. S. Rumsfeld, M. T. Roe, and E. D. Peterson, "Using digital health technology to better generate evidence and deliver evidence-based care," J. Am. Coll. Cardiol. **71**, 2680–2690 (2018).
8. D. Lupton, "Critical perspectives on digital health technologies," Soc. Compass **8**, 1344–1359 (2014).
9. C. L. Campbell and C. Besselli, "Impacting healthcare outcomes: connecting digital health within the veteran's health administration home-based primary care (HBPC) program," in *Three Facets of Public Health and Paths to Improvements* (2020), pp. 95–126.
10. R. Shan, S. Sarkar, and S. S. Martin, "Digital health technology and mobile devices for the management of diabetes mellitus: state of the art," Diabetologia **62**, 877–887 (2019).
11. Q. Shi, Z. Zhang, T. He, Z. Sun, B. Wang, Y. Feng, X. Shan, B. Salam, and C. Lee, "Deep learning enabled smart mats as a scalable floor monitoring system," Nat. Commun. **11**, 1 (2020).
12. R. Won, "Intelligent learning with light," Nat. Photonics **12**, 570–571 (2018).
13. K. Peters, "Polymer optical fiber sensors—a review," Smart Mater. Struct. **20**, 013002 (2011).
14. A. Leal-Junior and A. Frizera-Neto, *Optical Fiber Sensors for the Next Generation of Rehabilitation Robotics* (Elsevier, 2022).
15. T. Islam, S. C. Mukhopadhyay, and N. K. Suryadevara, "Smart sensors and Internet of Things: a postgraduate paper," IEEE Sens. J. **17**, 577–584 (2017).
16. S. Li, L. D. Xu, and S. Zhao, "5G Internet of Things: a survey," J. Ind. Inf. Integr. **10**, 1–9 (2018).
17. L. Avellar, C. S. Filho, G. Delgado, A. Frizera, E. Rocon, and A. Leal-Junior, "AI-enabled photonic smart garment for movement analysis," Sci. Rep. **12**, 4067 (2022).
18. A. G. Leal-Junior, C. A. Diaz, L. M. Avellar, M. J. Pontes, C. Marques, and A. Frizera, "Polymer optical fiber sensors in healthcare applications: a comprehensive review," Sensors **19**, C1–C30 (2019).
19. D. Li, "5G and intelligence medicine—how the next generation of wireless technology will reconstruct healthcare?" Precis. Clin. Med. **2**, 205–208 (2019).
20. G. Rajan, *Optical Fiber Sensors: Advanced Techniques & Applications* (CRC Press, 2015).
21. G. Numata, N. Hayashi, M. Tabaru, Y. Mizuno, and K. Nakamura, "Ultra-sensitive strain and temperature sensing based on modal interference in perfluorinated polymer optical fibers," IEEE Photon. J. **6**, 6802306 (2014).
22. A. Minardo, R. Bernini, and L. Zeni, "Distributed temperature sensing in polymer optical fiber by bofda," IEEE Photon. Technol. Lett. **26**, 387–390 (2014).
23. A. G. Leal-Junior, C. R. Díaz, C. Marques, M. J. Pontes, and A. Frizera, "Multiplexing technique for quasi-distributed sensors arrays in polymer optical fiber intensity variation-based sensors," Opt. Laser Technol. **111**, 81–88 (2019).
24. K. Hill and G. Meltz, "Fiber Bragg grating technology fundamentals and overview," J. Lightwave Technol. **15**, 1263–1276 (1997).
25. V. V. Spirin, P. L. Swart, A. A. Chtcherbakov, S. V. Miridonov, and M. Shlyagin, "20-km-length distributed fiber optical loss sensor based on transmission-reflection analysis," Opt. Eng. **44**, 040501 (2005).
26. M. K. Barnoski, M. D. Rourke, S. M. Jensen, and R. T. Melville, "Optical time domain reflectometer," Appl. Opt. **16**, 2375–2379 (1977).
27. W. Eickhoff and R. Ulrich, "Optical frequency domain reflectometry in single-mode fiber," Appl. Phys. Lett. **39**, 693–695 (1981).
28. D. Tosi, C. Molardi, M. Sypabekova, and W. Blanc, "Enhanced backscattering optical fiber distributed sensors: tutorial and review," IEEE Sens. J. **21**, 12667–12678 (2021).
29. V. Spirin, M. Shlyagin, S. Miridonov, and P. Swart, "Transmission/reflection analysis for distributed optical fibre loss sensor interrogation," Electron. Lett. **38**, 117–118 (2002).
30. V. Spirin, F. Mendieta, S. Miridonov, M. Shlyagin, A. Chtcherbakov, and P. Swart, "Localization of a loss-inducing perturbation with variable accuracy along a test fiber using transmission-reflection analysis," IEEE Photon. Technol. Lett. **16**, 569–571 (2004).
31. M. Cen, V. Moeyaert, P. Mégret, and M. Wuilpart, "Localization and quantification of reflective events along an optical fiber using a bi-directional TRA technique," Opt. Express **22**, 9839–9853 (2014).
32. M. Silveira, A. Frizera, A. Leal-Junior, D. Ribeiro, C. Marques, W. Blanc, and C. A. R. Díaz, "Transmission–reflection analysis in high scattering optical fibers: A comparison with single-mode optical fiber," Opt. Fiber Technol. **58**, 102303 (2020).
33. W. Blanc, I. Martin, H. Francois-Saint-Cyr, X. Bidault, S. Chaussedent, C. Hombourger, S. Lacomme, P. L. Coustumer, D. R. Neuville, D. J. Larson, T. J. Prosa, and C. Guillermier, "Compositional changes at the early stages of nanoparticles growth in glasses," J. Phys. Chem. C **123**, 29008–29014 (2019).

34. A. G. Leal-Junior, D. Ribeiro, L. M. Avellar, M. Silveira, C. A. R. Diaz, A. Frizera-Neto, W. Blanc, E. Rocon, and C. Marques, "Wearable and fully-portable smart garment for mechanical perturbation detection with nanoparticles optical fibers," IEEE Sens. J. **21**, 2995–3003 (2021).
35. W. Blanc, V. Mauroy, L. Nguyen, B. N. S. Bhaktha, P. Sebbah, B. P. Pal, and B. Dussardier, "Fabrication of rare earth-doped transparent glass ceramic optical fibers by modified chemical vapor deposition," J. Am. Ceram. Soc. **94**, 2315–2318 (2011).
36. L. Shiloh, A. Lellouch, R. Giryes, and A. Eyal, "Fiber-optic distributed seismic sensing data generator and its application for training classification nets," Opt. Lett. **45**, 1834–1837 (2020).
37. Y. Shi, Y. Wang, L. Wang, L. Zhao, and Z. Fan, "Multi-event classification for Φ-OTDR distributed optical fiber sensing system using deep learning and support vector machine," Optik **221**, 165373 (2020).
38. Y. Shi, Y. Wang, L. Zhao, and Z. Fan, "An event recognition method for Φ-OTDR sensing system based on deep learning," Sensors **19**, 3421 (2019).
39. Z. Sun, K. Liu, J. Jiang, T. Xu, S. Wang, H. Guo, Z. Zhou, K. Xue, Y. Huang, and T. Liu, "Optical fiber distributed vibration sensing using grayscale image and multi-class deep learning framework for multi-event recognition," IEEE Sens. J. **21**, 19112–19120 (2021).